Simulation of rolling contact fatigue strength for traction drive elements (comparison with fatigue test)

Simulation of rolling contact fatigue strength for traction drive elements (comparison with fatigue test)

Yukihito NARITA*, Masashi YAMANAKA**, Toshiharu KAZAMA*,
Yasuhiro OSAFUNE* and Tomoya MASUYAMA***
*Muroran Institute of Technology,
27-1 Mizumoto-cho, Muroran 050-8585, Japan
E-mail: y-narita@mmm.muroran-it.ac.jp
**High Energy Accelerator Research Organization,
1-1 Oho, Tsukuba, Ibaraki 305-0801, Japan
***Tsuruoka National College of Technology,
104 Inooka-sawada, Tsuruoka, Yamagata 997-8511, Japan

Received: 20 September 2017; Revised: 9 December 2017; Accepted: 31 January 2018

Abstract

A simulation of the rolling contact fatigue strength of a traction drive element was developed. This simulation accounts for both the distribution of sizes of inclusions in the element material and the influence of traction forces at the element surface. The shear strength of the matrix structure surrounding an inclusion was estimated with an equation. The purpose of this report is verifying the estimation accuracy of this simulation by comparing with the experimental result. The experiment was carried out by according to the 14 S-N testing method. The material of test rollers was carburized JIS SCM420H. The hardness distribution and the Weibull distribution of inclusion dimensions, which are necessary parameters of this simulation, were determined by observation of an actual test specimen. The calculated rolling contact fatigue strength in failure rate of 50% at 10^7 cycles was 750 MPa with a standard deviation of 35.4 MPa. The rolling contact fatigue strength of 1120 MPa with a standard deviation of 50.8 MPa was obtained as a result of experiment. The failure mode was considered to be flaking from the internal origination. The calculated standard deviation was about equal to the experimental result. Though there was 370 MPa difference between calculated and experimental fatigue strength. Including of the hardening of roller and the influence of compressive residual stress in the simulation and the determination of the depth of failure initiation will decrease above error.

Keywords : Machine element, Traction drive, Rolling contact fatigue, 14 S-N testing method, Inclusion, Tribology, Shear stress

1. Introduction

A traction drive transmits power through shear forces in the elastohydrodynamic lubrication film between pairs of rollers. Since contact forces play an integral role in traction drives for power transmissions, high contact pressures occur at the points of contact between rollers. For example, toroidal CVTs for automobiles are operated at maximum Hertzian pressure exceeding 4 GPa (Machida et al., 1995). These high contact pressures cause failure through rolling contact fatigue, which occurs in bearings and gears. The most common mode of failure is surface flaking. Therefore, prediction of the rolling contact fatigue strength is essential during the design of a traction drive.

A number of studies have reported the fatigue strength in traction drives. Many kinds of fatigue tests have been carried out on rollers and balls to examine the influence of failure mechanisms, operating conditions, lubrication modes, roller materials, etc., on fatigue strength (Machida et al., 1993; Deng et al., 1999; Nakajima and Mawatari, 2005; Matsuo et al., 1991; Coy et al., 1981; Rohn et al., 1981). Murakami (2002) proposed an equation for predicting the fatigue limit, which considers the size of microdefects or inclusions. Yamanaka et al. (2012) proposed a prediction equation for estimating the rolling contact fatigue strength of traction drive elements by extending Murakami's method.

It is well known that the high-strength materials employed in traction drives and gears show high scatter in fatigue strength (Murakami et al., 1988). A large number of fatigue tests must be performed to estimate the scatter. It would be very useful for strength design if the scatter could be estimated by simulation. The authors developed a simulation analysis of the rolling contact fatigue strength of traction drive elements (Narita et al., 2013, 2014) by accounting for both the distribution of sizes of inclusions in the element material and the influence of traction forces employing Masuyama's method (2002a, 2002b). Though, the verification of estimation accuracy is untouched. In order to do this, some experimental results of fatigue test are necessary. Although, this proposed simulation adopts Yamanaka's equation (2012), its evaluated stress is different from the Hertzian pressure adopted in other reports. Accordingly, the experimental results of previous research cannot be compared with this simulation.

Therefore, in this research, the rolling contact fatigue strength and the scatter at the 10^7 cycles are obtained by according to the 14 S-N rolling contact fatigue test by using two roller fatigue tester. And the result of simulation is compared with above experimental result.

2. Criterion of rolling contact fatigue

During rolling contact fatigue, cracks propagate parallel to the rolling direction. Therefore, as in previous research, we again concentrated on the shear stress parallel to the rolling direction, τ_{zx}. These cracks initiate from the inclusions and defects within the material and propagate to the point of failure by this τ_{zx}. This study uses the following criteria for the failure from a given defect in a traction drive element: rolling contact fatigue strength τ_w is assumed around a defect, and failure is assumed to occur if the shear stress τ_{zx} due to the contact force F_c, which is normal to the contact point, exceeds τ_w. The prediction equation for τ_w, defined as the rolling contact fatigue strength for 10^7 cycles, is given below (Yamanaka et al., 2012):

$$\tau_w = c \times \frac{1.56(Hv + 120)}{\left(\sqrt{area}\right)^{1/6}} \tag{1}$$

where Hv is Vickers hardness and $area$ is the projected area of an inclusion onto a plane perpendicular to the evaluation stress. Coefficient c is assigned the value 0.97 on the basis of the rolling contact fatigue strength found in a preliminary experiment using rollers with artificially induced defects of determined dimensions.

3. Simulation of rolling contact fatigue strength for traction drive elements

3.1 Simulation procedure

Figure 1 is a flow chart of the proposed simulation of the rolling contact fatigue strength of the traction drive elements (Narita et al., 2014). We begin by constructing the simulated virtual roller. "Virtual roller" means a computer model of a roller containing the same distribution of inclusions and surface hardness as an actual roller. As shown in Fig.2, this virtual roller model is created by combining the two-dimensional layers in the axial direction. Masuyama et al. (2002b) assumed an isotropic distribution of inclusions when evaluating the bending fatigue strength of a tooth root of a carburized gear in a simulation, and approximated the distribution of inclusions in the tooth width direction by combining two-dimensional virtual gear models in layers. The same method was used in this study.

First, inclusions are distributed in each layer of the virtual roller. Figure 3 is a histogram of the inclusion sizes determined by the observation of a specimen. A test specimen was made of pre-quenched Japan Industrial Standard (JIS) SCM420H. The bar stock, used to build the test rollers described below, was cut with a fine cutter and buffed to create the specimen. The number of inclusions and the surface area of each inclusion on the surface of the specimen were measured under a digital microscope (Keyence VH-8000, 2.11 megapixels). A total of 600 mm^2 of surface was examined. According to the research on SUJ2 by Murakami (2000), inclusions less than $\sqrt{area}$ = 2 μm do not affect the fatigue life of a roller; that is, such inclusions do not become the initiation sites of failure. In view of that report and the limits of precision of the digital microscope, we decided not to measure inclusions less than the size of 1 μm^2. It should be noted that the greater the inclusion size, the lower the frequency of occurrence. This distribution of inclusion

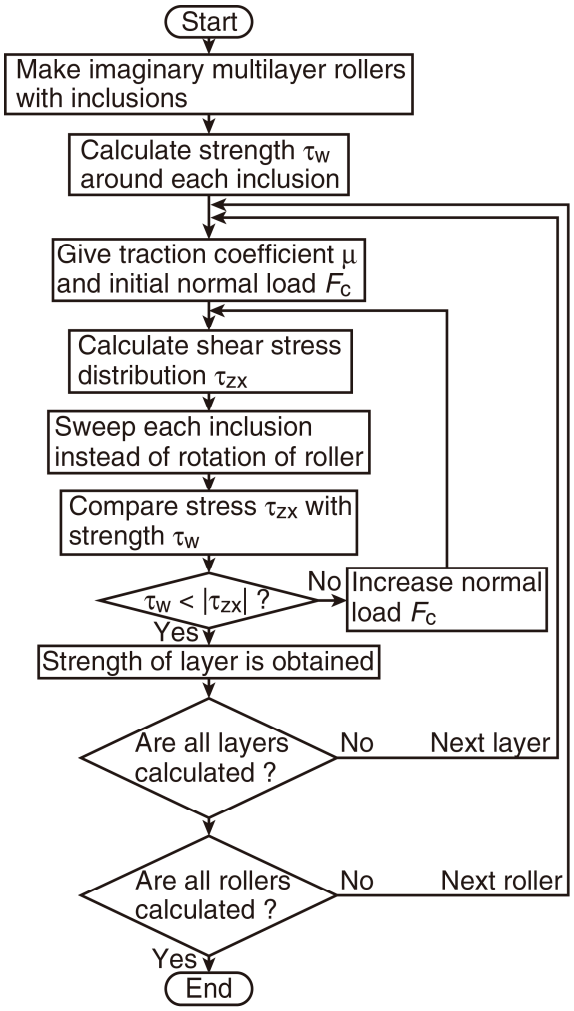

Fig. 1 Flow chart of simulation.

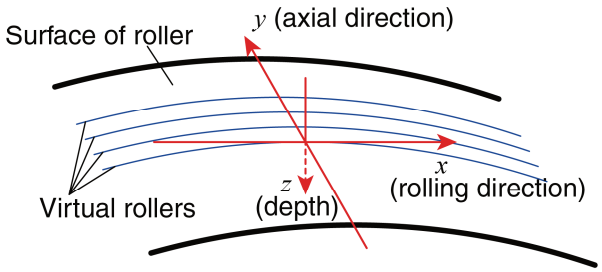

Fig. 2 Schematic and coordinates of virtual multilayered roller. Each layer contains same distribution of inclusions as an actual roller.

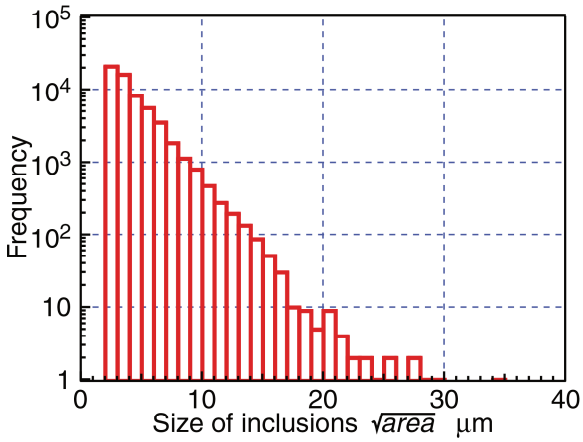

Fig. 3 Histogram of size of observed inclusions in bar stock of JIS SCM420H used to build test rollers.

dimensions followed a composite Weibull distribution. The following equations provide the composite Weibull distribution:

$$Y_1 = \ln\left(\ln\frac{1}{1-F(t)}\right) = m_1 \ln t - m_1 \ln \eta_1 \qquad (0 < F(t) < \delta) \tag{2}$$

$$Y_2 = \ln\left(\ln\frac{1}{1-F(t)}\right) = m_2 \ln t - m_2 \ln \eta_2 \qquad (\delta < F(t) < 1) \tag{3}$$

where $F(t)$ is the cumulative distribution percentage, m is the shape parameter, η is the scale parameter, and δ is the separation parameter. In this study, the Weibull random number was $t = \sqrt{area}$. As can be seen from the equations, the plot of Y with respect to $\ln t$ is a linear function. We can obtain m and η from the slope of the line and the intercept, respectively. The separation parameter δ in Eqs. (2) and (3) can be found by using intersection t_c of the two above lines:

$$t_c = \frac{m_1 \ln \eta_1 - m_2 \ln \eta_2}{m_1 - m_2} \tag{4}$$

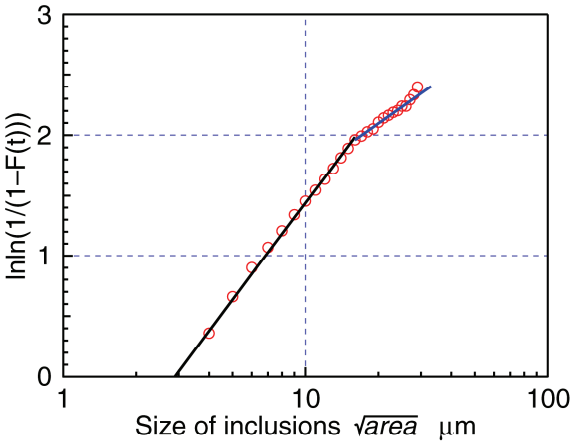

Fig. 4 Weibull plot of distribution of inclusions shown in Fig.3. Its parameters are presented in Table 1.

Table 1 Weibull parameters.

Weibull parameter m_1	1.158
Weibull parameter m_2	0.611
Weibull parameter η_1	2.886
Weibull parameter η_2	0.648
Boundary t_c	15.34
Density of inclusions [/mm^2]	100

Figure 4 combines the Weibull plot of the measured inclusion area $\sqrt{area}$ shown in Fig. 3 and the linear approximations of these results obtained from Eqs. (2) and (3). Table 1 provides the Weibull parameters obtained from the linear approximations. To obtain the reciprocal functions of Eqs. (2) and (3), we find:

$$t = \eta\left[-\ln\left(1-F(t)\right)\right]^{\frac{1}{m}} \tag{5}$$

Uniform random numbers were applied in $F(t)$ over the semi-open interval [0,1) to numerically obtain the Weibull random number $t = \sqrt{area}$. These random numbers were used to randomize the locations of the inclusions. This process allowed us to create virtual rollers that have the distribution of inclusion dimensions and density found in the actual material. Inclusions were placed in each layer of the virtual roller by the same method, and their locations were recorded in terms of depth z beneath the roller surface and angular location θ in the circumferential direction. It must be noted that in a few rare cases, huge inclusions were generated. These inclusions lowered the fatigue strength. In such cases, the maximum value $\sqrt{area}_{\max}$ = 51.6 μm for the inclusion area was estimated with the statistics of extremes (Murakami, 2002) and used as the upper limit of the $\sqrt{area}$ of generated inclusions (Narita et al., 2013).

The spacing between each layer in virtual roller is set at the mean distance between inclusions so that the model would be equal to the inclusion density of the actual material. The determined inclusion density from the observation of a specimen was 100/mm^2. The mean distance between inclusions calculated from this density is 0.1 mm. On this basis, the layer spacing in the virtual roller was set at 0.1 mm.

Using Eq. (1), we next calculate the rolling contact fatigue strength in the vicinity of an inclusion. For hardness Hv, required in this equation, we applied the values observed from the actual rollers before use for the fatigue test. The material was carburized SCM420H. Figure 5 presents the measured hardness in the depth direction. The maximum hardness H_2 was 725 Hv, and it occurred at a depth of d_2 = 0.15 mm below the roller surface. The surface hardness H_1 was 667 Hv, the core hardness H_3 was 430 Hv, and the effective case depth d_{eff} was 0.7 mm. We applied the approximated hardness at any depth z (Narita et al., 2013) obtained from observation of actual rollers:

$$Hv = \left(H_2 - H_3\right)\exp\left\{-A\left(z-d_2\right)^2\right\} + H_3 \tag{6}$$

$$\begin{cases} A = -\dfrac{1}{{d_2}^2}\ln\left(\dfrac{H_1 - H_3}{H_2 - H_3}\right) & \left(d \le d_2\right) \\ A = -\dfrac{1}{\left(d_{\text{eff}} - d_2\right)^2}\ln\left(\dfrac{550 - H_3}{H_2 - H_3}\right) & \left(d > d_2\right) \end{cases} \tag{7}$$

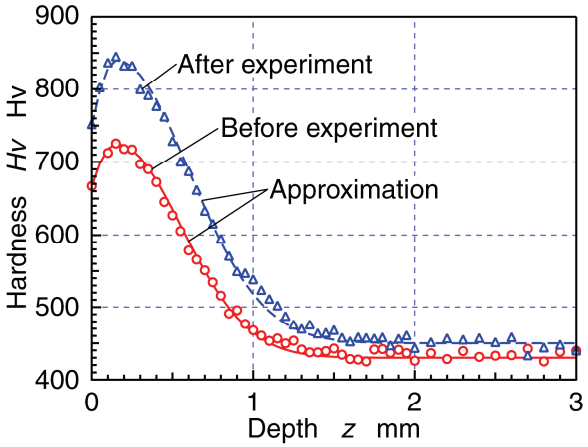

Fig. 5 Measured and approximated Vickers hardness of test roller made from carburized SCM420H.

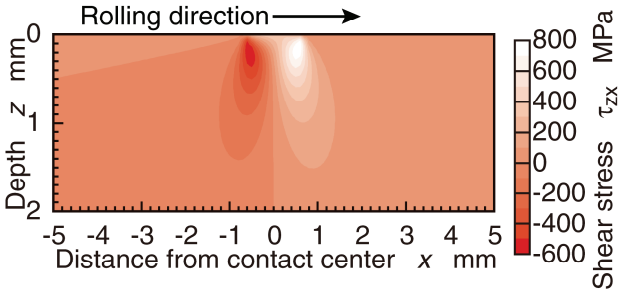

Fig.6 Distribution of shear stress τ_{xz} of driven roller under friction coefficient $\mu = 0.12$ ($F_c = 1800$ N). τ_{xz} in $x > 0$ region increases under traction force.

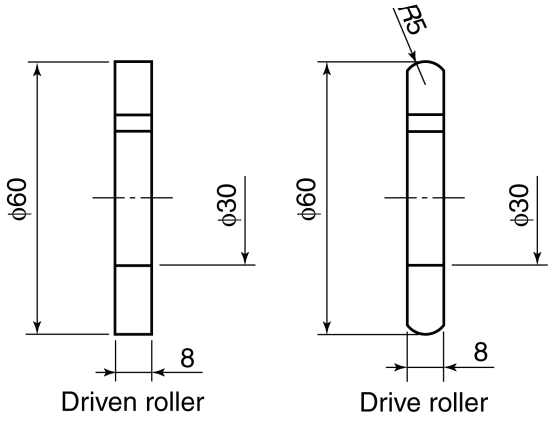

Fig.7 Shape and dimension of test roller pair for simulation and experiment

The approximated curve of hardness *Hv* according to Eqs. (6) and (7) is also shown in Fig.5.

Next, the shear stresses τ_{zx} occurring in each layer of the virtual roller are calculated by using the commercial boundary element method program TED/CPA (TriboLogics Corporation) (Kakoi 1991). This program can calculate the internal stresses in the roller occurring from frictional forces at the surface. Here, the friction coefficient, $\mu = 0.12$, was set equal to the traction coefficient found in an experiment (Yamanaka et al., 2012). Young's modulus of the roller material SCH420H is 207.5 GPa and Poisson's ratio is 0.3. Particularly high stresses occur in the vicinity of the contact point in Hertzian contact. To reduce the execution time, calculations were only carried out for the inclusions distributed in the virtual roller within a depth of $z \le 2$ mm below the roller surface. The calculation region for the stress distribution was placed with its origin at the contact point in the area $0 \le z \le 2$ mm in the depth direction and $-5 \le x \le 5$ mm in the rolling direction. Rolling was in the positive x direction. The increments in the x and z directions were 0.025 mm and 0.005 mm, respectively. The coordinate system is shown in Fig. 2. Figure 6 provides an example of the distribution of τ_{zx} at $y = 0$ under the contact force $F_c = 1800$ N. The roller was the same shape as those used in the experiment as shown in Fig. 7. The test rollers were cylindrical with a diameter of 60 mm. The drive roller had a crowning radius r_c of 5 mm and the driven roller was flat. The vertical scale in Fig. 6 is double that of the horizontal scale. This figure shows that τ_{zx} increases in the $x > 0$ region under traction force.

Finally, instead of rotating the roller, each inclusion is shifted toward the rolling direction in the stress distribution and the rolling contact fatigue strength τ_w, calculated in Eq. (1), is compared with τ_{zx}. Since the sign of τ_{zx} changes about the roller contact point, $|\tau_{zx}|$ is compared. Failure is assumed to occur when $\tau_w < |\tau_{zx}|$, and the fatigue strength for that case is recorded. When failure occurs from multiple inclusions, the inclusion with the lowest τ_w is designated as the failure initiation site. When no failure occurs, the contact force F_c is increased, the stress distribution is re-calculated, and the comparison of the fatigue strength with $|\tau_{zx}|$ is repeated. Once failure occurred, it is transmitted to the

neighboring layers, and the above procedure is repeated for all layers. The layer with the lowest F_c at the time of failure is then designated the failure initiation site in the virtual roller. This process is repeated for a given number of simulated rollers, and histograms of the fatigue strength are output.

3.2 Results of simulation

We carried out above simulation of the rolling contact fatigue strength. For this simulation, 1000 virtual rollers were created. The calculations were carried out while increasing the contact force F_c in steps of 50 N.

Figure 8 is a histogram of the rolling contact fatigue strength τ_w obtained in the simulations. Here, τ_w was distributed between 650 and 840 MPa with a standard deviation σ = 35.4 MPa. Figure 9 is a normal probability plot of the results. The figure shows these points in a linear curve, thus indicating that the results of the simulation approximately obey a normal distribution. The rolling contact fatigue strength resulting in a failure rate of 50% was calculated at 750 MPa.

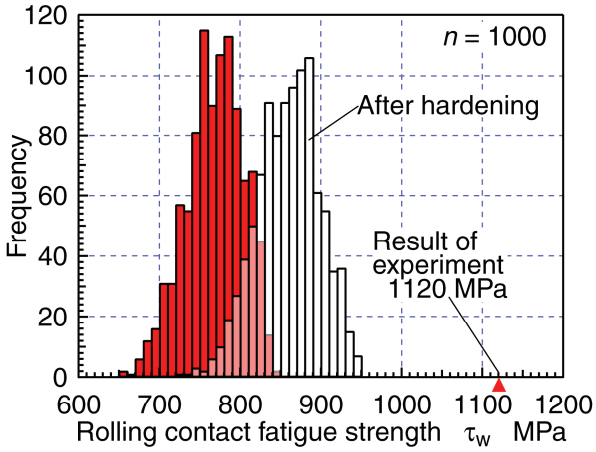

Fig. 8 Estimated rolling contact fatigue strength by simulation and result of 14 S-N testing metod at 10^7 cycles.

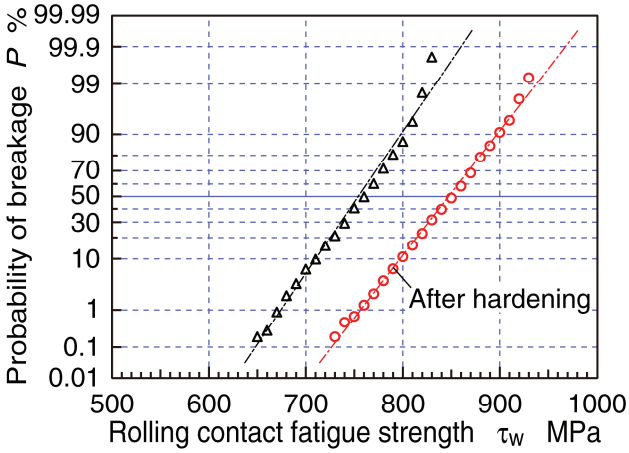

Fig. 9 Normal probability plot of estimated rolling contact fatigue strength by simulation. Results of simulation approximately obey normal distribution.

4. Rolling contact fatigue test of traction drive elements by two roller fatigue tester

4.1 Condition of experiment

Figure 10 shows the schematic of two roller fatigue tester employed in the experiment for obtaining S-N curve of traction drive elements. The driven roller box mounted on the slide base can move to the radial direction of driven roller. The loading arm pushes the rear of driven roller box, and a pair of rollers is pressurized under the given contact force. Traction oil (ITF32, Idemitsu Kosan Co. Ltd.) is supplied to the contact point of rollers. The temperature of oil is adjusted to 313±5 K. Through the toothed belt, the three-phase induction motor under the base plate drives a drive roller fixed on the input shaft. The rated speed of motor is 3000 min^{-1}. The input shaft also drives the reduction gear pair having a gear ratio of 45:46. Thus the rotational speed of driven roller become 2% slower than the drive roller. The proximity sensor mounted beside the driven shaft counts the revolution number of driven roller. When a failure of roller occurs, the acceleration sensor of driven roller box detects the vibration and the rotation of motor stops.

The shape of test rollers as shown in Fig. 7 and the bar stock used to build them are same as those used in the simulation. The material was carburized SCM420H. To make the same quenching conditions, all rollers were quenched at once. The measured hardness was shown in Fig.5. The compressive residual stress on the surface of rollers were 300 to 350 MPa. The surface roughness of rollers were Ra = 0.02 to 0.03 μm. Under the condition of below experiment, the minimum oil film thickness calculated by Hamrock-Dowson's equation is more than 0.23 μm. Therefore the oil film thickness is sufficiently thick for a traction drive.

According to the 14 S-N testing method (JSME, 1994), we estimate the rolling contact fatigue strength at the 10^7 cycles. The evaluation stress is maximum shear stress $\tau_{zx\,max}$. This value is calculated by TED/CPA (Kakoi 1991) under the given loading force. The step of $\tau_{zx\,max}$ is 45 MPa.

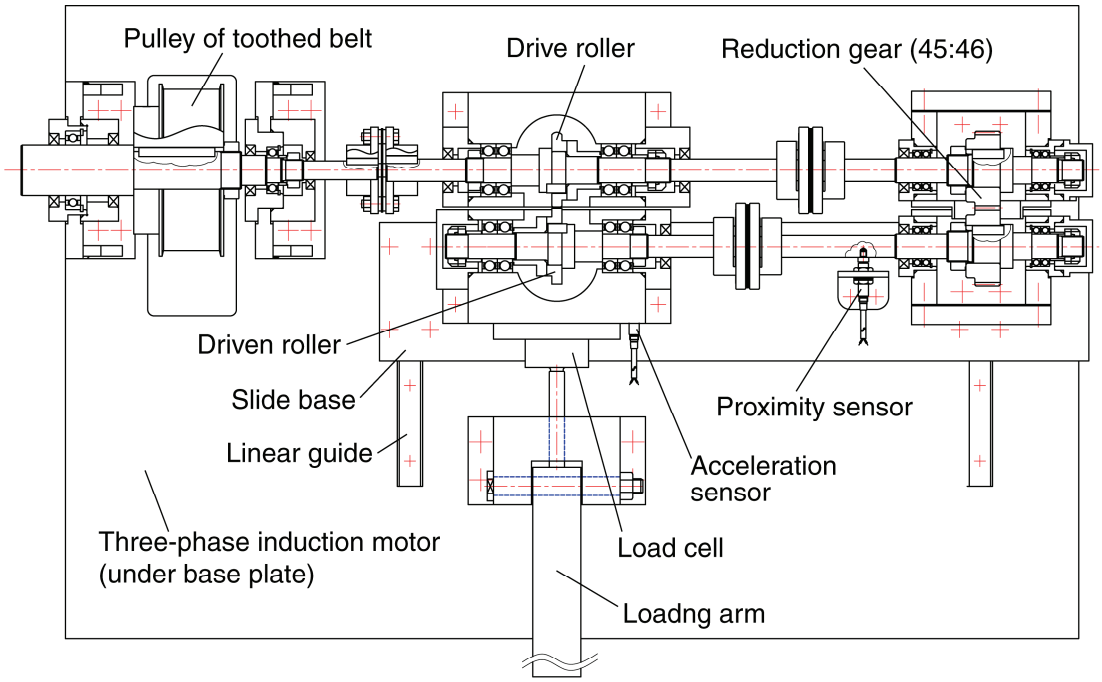

Fig.10 Schematic of two roller fatigue tester employed in experiment for obtaining S-N curve.

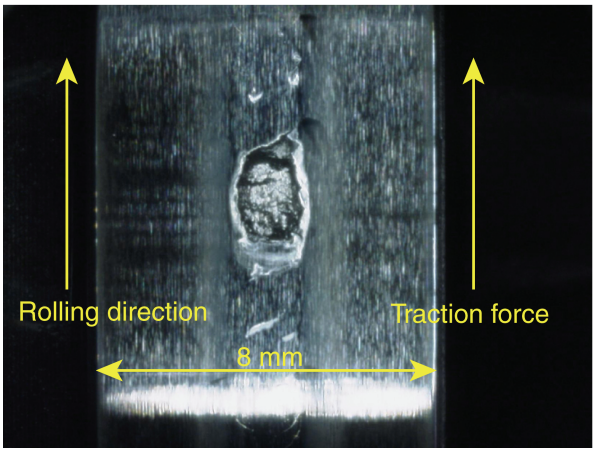

Fig.11 Photograph of failure point on failed test roller at $\tau_{zx\ max}$ = 1154 MPa and $N = 5.98\times10^6$ cycles.

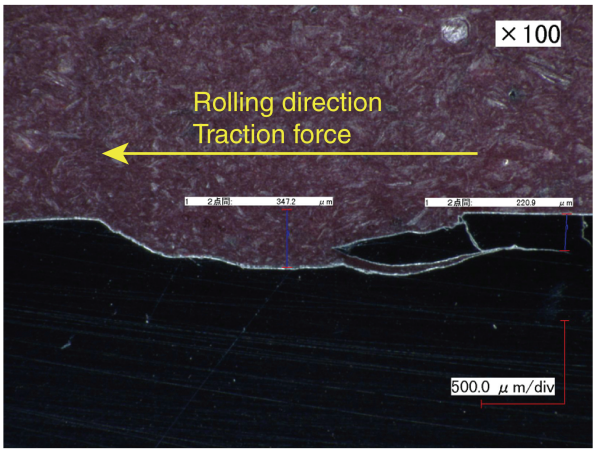

Fig.12 Cross section photograph of failure point shown in Fig.11.

4.2 Results of experiment

Figure 11 is the photograph of failed test roller at $\tau_{zx\ max}$ = 1154 MPa and $N = 5.98\times10^6$ cycles. We can see a kind of flaking of several mm^2. No cracks and pits was observed before this failure occurred. The upper and lower scars surrounding this failure point were caused by the inertial rotation of motor; that is, the failure point on test roller impacts the other roller, and the damaged point on this roller impacts the failed roller again. An equal interval scars from 2% slip of test rollers support above fact. Figure 12 is the cross section of the failure point. A subsurface crack propagated toward rolling direction, and a part of it flaked away. Therefore, the failure mode of this experiment was considered to be flaking from the internal origination. The appearances of failure point on another roller were similar to the mentioned above, and the depth of flaking was in the range of 0.1 to 0.5 mm.

Figure 13 shows the relation between maximum shear stress $\tau_{zx\ max}$ and fatigue life N. The marker with arrow indicate that the no failure occurred up to 10^7 cycles. The straight line is the regression line (JSME, 1994) derived from experimental results:

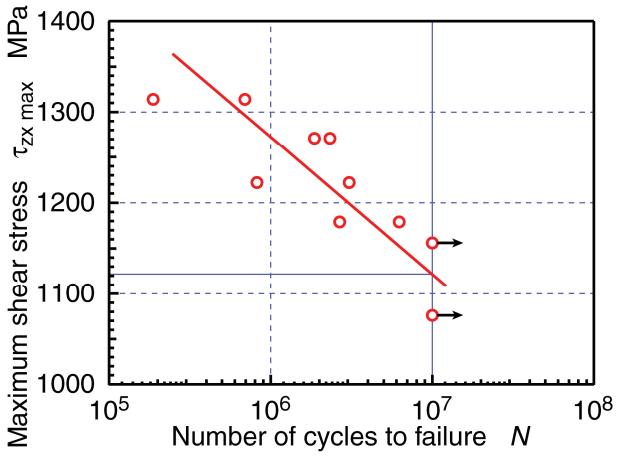

Fig.13 Obtained S-N curve according to 14 S-N testing method. Fatigue strength in failure rate of 50% at $N = 10^7$ cycles is 1120 MPa with standard deviation of 50.8 MPa.

$$\log N = \hat{\alpha} + \hat{\beta} S \tag{8}$$

Where S is the stress, and:

$$\hat{\alpha} = \overline{\log N} - \hat{\beta}\overline{S} \tag{9}$$

$$\hat{\beta} = \frac{\sum_{i=1}^{8}\left(S_i - \overline{S}\right)\left(\log N_i - \overline{\log N}\right)}{\sum_{i=1}^{8}\left(S_i - \overline{S}\right)^2} \tag{10}$$

$$\overline{\log N} = \frac{1}{8}\sum_{i=1}^{8}\log N_i \tag{11}$$

$$\overline{S} = \frac{1}{8}\sum_{i=1}^{8} S_i \tag{12}$$

Equation 8 indicates $\tau_{zx\,max}$ = 1120 MPa as the fatigue strength in failure rate of 50% at $N = 10^7$ cycles. The standard deviation of fatigue strength σ is calculated by (JSME, 1994):

$$\sigma = \frac{1}{\left|\hat{\beta}\right|}\sqrt{\frac{1}{6}\sum_{i=1}^{8}\left(\log N_i - \hat{\alpha} - \hat{\beta} S_i\right)^2} \tag{13}$$

Using this equation, we obtain σ = 50.8 MPa.

4.3 Comparison with calculated result

The calculated σ = 35.4 MPa was about equal to the experimental σ = 50.8 MPa. Though, there was 370 MPa difference between calculated τ_w = 750 MPa and experimental $\tau_{zx\,max}$ = 1120 MPa. It is thought that the error is caused by the following reasons.

In the experiment, we adopted $\tau_{zx\ max}$ as the evaluation stress because the depth of failure initiation was not determined. As shown in Fig.6, τ_{zx} changes with the depth z. If z is slightly away from the point of $\tau_{zx\ max}$, τ_{zx} shows several hundred MPa decrease. Therefore, the determination of the depth of failure initiation will reduce the difference from the calculated result.

Added to above, a plastic deformation of several μm was observed in the early stage of each fatigue test. This value has negligible influence on the shear stress distribution of rollers, but non-negligible effect on the hardness. Figure 5 also provide the measured hardness of test roller after the fatigue test. This result was obtained from the roller of which failed in the condition of $\tau_{zx\ max}$ = 1154 MPa. In this figure, we can see the increase of subsurface hardness, and particularly, the 115 Hv increase of maximum hardness. The maximum hardness H_2, the surface hardness H_1, and the core hardness H_3 were 840, 750 and 450 *Hv*, respectively. This result indicates that the phenomenon like the work hardening occurred under the contact force given to the rollers. Equation 1 predicts that τ_w is heightened as the hardness *Hv* increases. Figure 8 and 9 also shows the simulation result of τ_w by using the approximated hardness of after hardening by using Eqs. (6) and (7). The rolling contact fatigue strength resulting in a failure rate of 50% was calculated at 850 MPa, and the difference between simulation and experiment was reduced to 270 MPa. Therefore, including the hardening in the simulation will reduce the difference from the experimental result.

Furthermore, the current simulation does not consider the influence of compressive residual stress. As mentioned above, the compressive residual stress on the surface of test rollers were 300 to 350 MPa. Taking account of compressive residual stress into the simulation will reduce the difference from the experimental result. However, there is a possibility that the compressive residual stress will change with the depth from surface of roller. In order to improve the simulation, measurement of compressive residual stress in the depth direction is necessary.

5. Conclusions

The simulations of the rolling contact fatigue strength for traction drive elements was carried out, and the estimation accuracy of it was compared with the experimental result. The experiment was carried out by according to the 14 S-N testing method. The material of test rollers was carburized JIS SCM420H. The following results were obtained.

(1) The calculated rolling contact fatigue strength in failure rate of 50% at $N = 10^7$ cycles was 750 MPa with standard deviation of 35.4 MPa.
(2) The rolling contact fatigue strength of 1120 MPa with standard deviation of 50.8 MPa was obtained as a result of experiment. The failure mode was considered to be flaking from the internal origination.
(3) The calculated standard deviation was about equal to the experimental result. Though there was 370 MPa difference between calculated and experimental fatigue strength.
(4) Including of the hardening of roller and the influence of compressive residual stress in the simulation, and the determination of the depth of failure initiation will decrease above error.

Acknowledgement

This study was made possible by the research grant program by the JGC-S scholarship foundation (2016), a grant by Schaeffler Japan Co., Ltd. (2016), and a Grant-in-Aid for Scientific Research (Grant-in-Aid for Young Scientists (B), No.25820028, 2013 to 2015) by the Japan Society for the Promotion of Science. Idemitsu Kosan Co., Ltd. offered the traction oil. Nippon Steel & Sumitomo Metal Corporation offered the bar stocks. We offer our deep thanks for these assistance.

References

Coy, J. J., Rohn, D. A., and Loewenthal, S. H., Constrained fatigue life optimization of a Nasvytis multiroller traction drive, Transaction of the American Society of Mechanical Engineers, Journal of Mechanical Design, Vol. 103 (1981), pp. 423-428.

Deng, G., Yamanaka, M., Yamamoto, R., Ono, N., Kato, M., and Inoue, K., Contact fatigue and strength evaluation of traction drive rollers, Transactions of the Japan Society of Mechanical Engineers, Ser. C (in Japanese), Vol. 65,

No. 635 (1999), pp. 2880-2885.

JSME, “Standard Method of Statistical Fatigue Testing (2nd Edition)”, Maruzen (1994).

Kakoi, K., Numerical Analysis of 3-dimensional contact problems with friction by special boundary element method, Transactions of the Japan Society of Mechanical Engineers, Ser. A (in Japanese), Vol. 57, No. 544 (1991), pp. 3010-3015.

Machida, H., Itoh, H., Imanishi, T., and Tanaka, H., Design principle of high power traction drive CVT, SAE paper, 950675, (1995).

Machida, H., Hata, H., Nakano, M., and Tanaka, H., Half-toroidal traction drive continuously variable transmission for automobile propulsion systems (traction drive materials, transmission design and efficiency), Transactions of the Japan Society of Mechanical Engineers, Ser. C (in Japanese), Vol. 59, No. 560 (1993), pp. 1154-1160.

Masuyama, T., Asano, J., and Inoue, K., Fatigue strength simulation of carburized gears based on Weibull distribution of inclusions, Proc. JSME (in Japanese), No. 02-12 (2002a), pp. 33-36.

Masuyama, T., and Katsumi INOUE, Computation of fatigue strength of carburized gears based on simulated distribution of defects, Proceedings of International Conference on Gears, VDI-Berichte, Nr. 1665 (2002b), pp. 421 - 434.

Matsuo, K., Saeki, S., Ooue, Y., and Yoshida, A., Effect of traction fluid on rolling contact fatigue life of thermally refined steel, Tribology Series, Vol.18 (1991), pp. 445–450.

Murakami, H., Estimation of rolling contact fatigue life due to determination of non-metallic inclusions, NTN Technical Review (in Japanese), No. 68 (2000), pp. 58-62.

Murakami, Y., Metal fatigue: effects of small defects and nonmetallic inclusions, Elsevier, (2002).

Murakami, Y., Kodama, S., and Konuma, S., Quantitative evaluation of effects of nonmetallic inclusions on fatigue strength of high strength steel, Transactions of the Japan Society of Mechanical Engineers, Ser. A (in Japanese), Vol. 54, No. 500 (1988), pp. 688-696.

Nakajima, A., and Mawatari, T., Rolling contact fatigue life of bearing steel rollers lubricated with low viscosity traction oil, Tribology and Interface Engineering Series, Vol. 48 (2005), pp. 351-362.

Narita, Y., Yamanaka, M., Kazama, T., Osafune, Y., and Masuyama, T., Simulation of rolling contact fatigue strength for traction drive elements, Journal of Advanced Mechanical Design, System and Manufacturing, Vol.7, No.3 (2013), pp. 432-447.

Narita, Y., Kato N., Yamanaka, M., Kazama, T., Osafune, Y., and Masuyama, T., Effect of crowning radius on rolling contact fatigue strength for traction drive elements (Evaluation by simulation), Journal of Advanced Mechanical Design, System and Manufacturing, Vol.8, No.6 (2014), DOI: 10.1299/jamdsm.2014jamdsm0081.

Rohn, D. A., Loewenthal, S. H., and Coy, J. J., Simplified fatigue life analysis for traction drive contacts, Transaction of the American Society of Mechanical Engineers, Journal of Mechanical Design, Vol. 103 (1981), pp. 430-439.

Yamanaka, M., Yamamura, J., Narita, Y., and Inoue, K., Evaluation of rolling contact fatigue strength for traction-drive elements by using artificial defect, Journal of Japan Society for Design Engineering (in Japanese), Vol. 47, No. 5 (2012), pp. 252-258.